American Journal of Transplantation 2007; 7: 201–210
Blackwell Munksgaard

doi: 10.1111/j.1600-6143.2006.01584.x

Quilty Effect Has the Features of Lymphoid Neogenesis and Shares CXCL13–CXCR5 Pathway With Recurrent Acute Cardiac Rejections

E. Di Carlo[a,b,*], T. D'Antuono[a], S. Contento[a,b], M. Di Nicola[c], E. Ballone[c] and C. Sorrentino[a,b]

[a] *Department of Oncology and Neurosciences, Anatomic Pathology Section, 'G. d'Annunzio' University, Chieti, Italy*
[b] *Ce.S.I. Aging Research Center, 'G. d'Annunzio' University Foundation, Chieti, Italy*
[c] *Department of Biomedical Sciences, Laboratory of Biostatistics, 'G. d'Annunzio' University, Chieti, Italy*
* *Corresponding author: Emma Di Carlo, edicarlo@unich.it*

Quilty effect (QE) is a frequent, yet enigmatic feature of cardiac allograft, since it is apparently devoid of clinical significance, though its association with acute (A) rejection (R) is strongly suspected.

It was observed in 126/379 biopsies from 22 patients during the first posttransplant year. Most grade (G)2R biopsies displayed a concomitant QE. The following features typical of QE were identified: (a) focal angiogenesis and lymphangiogenesis associated with bFGF, VEGF-C and VEGF-A expression, (b) marked infiltrate of $CD4^+$T and $CD20^+$B followed by $CD8^+$ T lymphocytes arranged around $PNAd^+$HEV-like vessels. Most QE appear as distinct B–T-cell-specific areas with lymphoid follicles sometimes endowed with germinal center-like structures containing $VCAM\text{-}1^+CD21^+$FDC and $CD68^+$macrophages, which frequently expressed CXCL13. These cells were also found in mantle-like zones, where small lymphocytes expressed CXCR5, otherwise in the whole area of not clustered lymphoid aggregates. CXCL13 was also expressed, in association with $CD20^+$B lymphocyte recruitment, in G2R biopsies obtained from patients with recurrent AR.

QE has features of a tertiary lymphoid tissue suggesting an attempt, by the heart allograft, to mount a local response to a persistent alloantigen stimulation resulting in aberrant CXCL13 production, as also occurs in recurrent AR. CXCL13-CXCR5 emerge as a common molecular pathway for QE and recurrent episodes of AR.

Key words: Endomyocardial biopsy, graft-infiltrating lymphocytes, inflammation, transplantation

Received 3 July 2006, revised 31 August 2006 and accepted for publication 6 September 2006

Introduction

Twenty-five years after its identification in 1981, the QE, defined as mononuclear cell aggregation in endomyocardial biopsies (EMBs) of the transplanted heart, is still an enigma. Determination of its pathological significance requires answers to the following questions. Which molecular and cellular mechanisms lead to its development? Are some of these mechanisms shared with those of allograft rejection? The few, extremely controversial findings (1) are currently pointing to associations of QE with both acute (2,3) and chronic (4) rejection, though the mechanisms underlying these links are obscure. It thus seemed reasonable to suppose that investigations of the cellular and molecular aspects of the QE might help in understanding its real biological meaning. Thus, the goal of our study is to shed light on immunopathological events involved in the onset of QE to better characterize this lesion and look for its correlations with rejection episodes.

This article provides the first support for the view suggested by our and previous morphological observations (5–7), namely that QE has the features of ectopic lymphoid tissue. It also indicates that QE shares a common molecular and cellular pathway, consisting of CXCL13 (also called B cell attracting chemokine 1, BCA-1 or B Lymphocyte Chemoattractant**,** BLC) expression and $CD20^+$B lymphocyte recruitment, with recurrent episodes of acute rejection (AR).

Materials and Methods

Patients, tissue samples and histopathological analyses of EMBs

Twenty-two consecutive patients (18 males, 4 females) aged 50–66 years and transplanted for idiopathic dilated cardiomyopathy (16 patients) or ischemic cardiopathy (6 patients) were enrolled immediately after transplantation and followed for 1 year. All patients were monitored for AR through EMBs.

All biopsies were performed by trained hemodynamists at the Department of Cardiology, 'SS Annunziata' Hospital, Chieti, Italy, following catheterization of the jugular vein as part of a standard protocol for posttransplant monitoring and when rejection episodes were suspected.

Table 1: Antibodies used on paraffin-embedded sections

Antibody	Clone	Origin	Dilution	Source
BAFF	Buffy-2	Rat	1/100	Alexis (Lausen, Switzerland)
bFGF		Rabbit	1/50	Calbiochem (San Diego, CA, USA)
MAdCAM	MECA-367	Rat	1/30	BD (San Diego, CA, USA)
PNAd	MECA-79	Rat	1/100	BD (San Diego, CA, USA)
CD3	F7.2.38	Mouse	1/50	Dako
CD8	C8/144B	Mouse	1/30	Dako
CD15	C3D-1	Mouse	1/25	Dako
CD20	L26	Mouse	1/100	Dako
CD21	1F8	Mouse	1/100	Dako
CD23	MHM6	Mouse	1/100	Dako
CD31	JC70A	Mouse	1/30	Dako
CD68	PG-M1	Mouse	1/30	Dako
CD138	MI15	Mouse	1/100	Dako
D2-40	D2-40	Mouse	1/70	Dako
FDC	CNA.42	Mouse	1/50	Dako
vWF	F8/86	Mouse	1/40	Dako
CD57	NK-1	Mouse	1/50	Novocastra (Newcastle, UK)
CD83	1H4b	Mouse	1/5	Novocastra (Newcastle, UK)
CXCL13	53 610	Mouse	1/30	R&D (Minneapolis, MN, USA)
VEGF-A		Rabbit	1/300	Santa Cruz (Santa Cruz, CA, USA)
VEGF-C		Rabbit	1/400	Zymed (San Francisco, CA, USA)

A total of 379 EMBs were obtained during the year: 17 per patient plus 5 required in the light of the clinical assessment. Samples were collected weekly for 4 weeks, fortnightly until 12 weeks and then monthly. Six small biopsies were taken at each sampling time. Biopsies were analyzed by two pathologists, E.D.C. and C.S. There was an almost perfect agreement (kappa value = 0.82) between their gradings (8).

For histological studies, four biopsies were fixed in 4% formalin, embedded in paraffin, sectioned at 4 μm and stained with hematoxylin–eosin (H&E). For immunohistochemical and immunofluorescence studies, two biopsies were snap-frozen in liquid nitrogen. Paraffin-embedded and frozen biopsies were histopathologically examined for rejection and QE in accordance with the criteria established (9) and updated (10) in November 2005 by the International Society for Heart and Lung Transplantation (ISHLT): grade (G)0R 'no rejection' (no change from 1990); G1R 'mild rejection', (1990 G1A, G1B and G2); G2R 'moderate rejection', (1990 G3A); and G3R 'severe rejection', (1990 G3B and G4).

The QE presents as nodular endocardial infiltrates that may be confined to the endocardium (1990 ISHLT QE A) (9) or extend into the underlying myocardium where associated myocyte damage may be present (1990 ISHLT QE B) (9).

All patients received rabbit anti-thymocyte globulin, cyclosporine A, azathioprine and steroids at doses and intervals determined by the time since transplantation and the occurrence of rejection episodes (11). QE has been considered distinct from AR insofar as it requires no treatment in the form of intensified immunosuppression (10,11).

Written informed consent was obtained from patients and the study was approved by the Ethical Committee of the 'SS. Annunziata' Hospital and the Institutional Review Board of the 'G. d'Annunzio' University. This investigation conformed to the principles outlined in the Declaration of Helsinki.

We also used formalin-fixed, paraffin-embedded lymph node samples archived in the Anatomic Pathology Institute of Chieti, Italy, (histologic report of lymph node tissue with follicular hyperplasia and sinus histiocytosis) and endoscopic biopsies (histologic report of chronic, active Helicobacter pylori-induced gastritis with florid lymphoid follicles, according to the updated Sydney classification) (12).

Antibodies and immunohistochemistry

For immunohistochemistry on the formalin-fixed, paraffin-embedded samples, sections were treated with H_2O2 3% for 5 min to inhibit endogenous peroxidase and then washed in H_2O. Antigen was unmasked by treatment with EDTA at pH 9 (prior to incubation with anti-CD83, FDC, vWF, CXCL13 and D2-40 antibody [Ab]), or with citrate buffer at pH 6 (prior to incubation with anti-CD8, CD15, CD20, CD23, CD68, CD138 and PNAd Abs) in a microwave oven (two 5 min courses). The slices were then held for 20 min at room temperature. After washing in PBS/Tween-20, immunohistochemical staining was performed, as previously reported (13), with the primary Abs listed in Table 1.

For immunohistochemistry on the frozen samples, cryostat sections were fixed in acetone for 10 min.

After washing in PBS/Tween-20, sections were stained as reported (13) with the primary Abs listed in Table 2. Table 3 lists the antisera most useful for the scope of this study and the reasons for their applications on biopsies with QE.

Viral infections were tested on paraffin-embedded tissue sections according to published protocols (14,15). To test biopsies for complement components, the indirect immunofluorescence method was performed on acetone-fixed frozen sections as reported (16).

After immunohistochemical staining, automated cell counts (17) were performed on a Leica Imaging Workstation (Leica Microsystems, Wetzlar, Germany) by applying a dedicated algorithm in Qwin image analysis software (version 2.7). Because hematic and lymphatic capillaries may be identified as small tubes or circles marked by vWF or D2-40 Abs respectively, appropriate automated count was not feasible with the current software, thus they were counted by two pathologists in a blind fashion. The results (Figure 1, panel C and D) were expressed as the mean of their independent evaluations.

Table 2: Antibodies used on frozen sections

Antibody	Clone	Origin	Dilution	Source
CD209	DCN46	Mouse	1/100	BD
VCAM-1	51-10C9	Mouse	1/200	BD
CD4	MT310	Mouse	1/50	Dako
ICAM-1	6.5B5	Mouse	1/200	Dako
CXCR5	51 505	Mouse	1/100	R&D

Table 3: Antibodies most significant for the scope of this study and the meaning of their application on EMBs with QE

Antibodies	Usefulness of their application in QE
BAFF, CXCL13 and its receptor CXCR5	Reveal whether B lymphocyte recruitment in QE is associated with expression of powerful B lymphocyte attracting chemokines usually detected in lymphoid organs and playing a key role during lymphoid neogenesis
bFGF, VEGF-A, VEGF-C	Reveal whether the high microvessel density observed in most of QE is related to expression of the main angiogenic and lymphangiogenic factors
vWF, CD31	Reveal blood vessels and assess the nature of the numerous micro-channels developed in most QE
D2-40	Reveals lymphatics and assess whether they co-operate in the high microvessel density and massive lymphocyte accumulation of QE
PNAd	Reveals sialomucins constitutively expressed in lymphoid organ postcapillary venules and inducible by lymphoid chemokines during ectopic lymphoid neogenesis
CD21, CD23, CD35, FDC	Reveal the presence of follicular dendritic cells fundamental in sustaining germinal center reactions in lymphoid organs

Hematic and lymphatic capillary and leukocyte counts were performed by evaluating microvessel/cells in randomly chosen fields in the case of G0R EMBs, or in fields containing inflammatory foci consistent with the diagnosis of QE or G1R and G2R. To secure sufficient tissue for the analysis of numerous consecutive sections, QE were considered suitable for immunohistochemical analyses when their endocardial or endomyocardial infiltrate extended for >1.57 mm^2, and according to their histological features as will be described following (i.e. equal number between QE with or without follicular lymphocyte arrangement). Out of this criterion, biopsies (with QE or with rejection from G0R to G2R) were randomly chosen from all 22 patients after the exclusion of inadequate biopsy sets and biopsies positive for viral infections. Values are represented as the mean $\pm$ SD of positive microvessel-cells/field evaluated by light microscopy on single immunostained formalin-fixed paraffin-embedded (vWF, D2-40, CD68, CD83, CD8, CD20, CD138, CD57, CD15) or cryostat (CD209, CD4) sections at $\times$400 in a 85 431.59 μm^2 field. Three high-power fields were analyzed for each section and three sections per biopsy were evaluated.

Double immunohistochemical and immunofluorescent analyses

Double immunohistochemistry on paraffin-embedded tissue sections was performed with anti-CD68 and anti-CXCL13 Abs, by using the EnVision™ G/2 Doublestain System, Rabbit/Mouse (Dako, Glostrup, Denmark) according to the manufacturer's protocol and analyzed under a Leica DMLB light microscope. Double immunofluorescent staining on acetone-fixed frozen sections was performed with anti-CD21 and anti-VCAM-1 Abs, as previously reported (18) and analyzed under a Zeiss LSM 510 Meta confocal microscope (Zeiss, Oberkochen, Germany).

Statistical analysis

Data were reported as mean and standard deviation (SD). Differences between groups of EMB for hematic microvessel density and lymphatic microvessel density were assessed by one-way analysis of variance (ANOVA) test. The difference between each pair of means was evaluated with the Tukey pairwise multiple comparisons test. Differences between reactive cells in groups of EMB with G0R or QE were evaluated with the Mann–Whitney *U* test.

All statistical tests were evaluated at an α level of 0.05. Statistical analysis was carried out with SPSS software, version 11.0 (SPSS Inc, Chicago, IL, USA).

Results

Morphological features of QE

The QE was observed in 126 EMBs (33.2% of the total of 379) from 16 patients: 108 from 14 males, 18 from 2 females. The rejection grades were: 170 G0R (22/22 patients), including 29 (17%) with QE; 182 G1R (22/22 patients), including 83 (45.6%) with QE; 25 G2R (14/22 patients), including 14 (56%) with QE; 2 G3R (2/22 patients), none with QE. A nonsignificant association was found with the Mann–Whitney *U* or the chi-square test, between patients who did or did not develop QE and variables such as host and donor age, host weight and diagnosis prior to transplantation.

EMBs with QE showed aggregates of lymphomononuclear cells confined to the endocardium or invading the underlying myocardium. All the extensive infiltrates (>1.57 mm^2) displayed the peculiar features illustrated in Figure 1: a) high-microvessel density confined to the QE (panel A, arrows); b) plumping of most of the microvascular endothelium, occasionally similar to the cuboidal appearance of the high-endothelial venule (HEV) of lymphoid tissues (panel A, arrowheads and inset).

Furthermore, in 77 QE (about 61%) the endomyocardial infiltrate was arranged in lymphoid follicles in various stages of development. Some of the wider infiltrates displayed secondary follicles endowed with germinal center-like structures (12/ 126, i.e. 9.5%) as represented in Figure 1, panel A. These features recall the lymphoid tissue microarchitecture. They are absent in G0R and all grades of AR. The cellular and molecular profile of the quilty infiltrate was therefore searched for features common to AR, since (a) most of G2R EMBs displayed the QE, (b) most of these

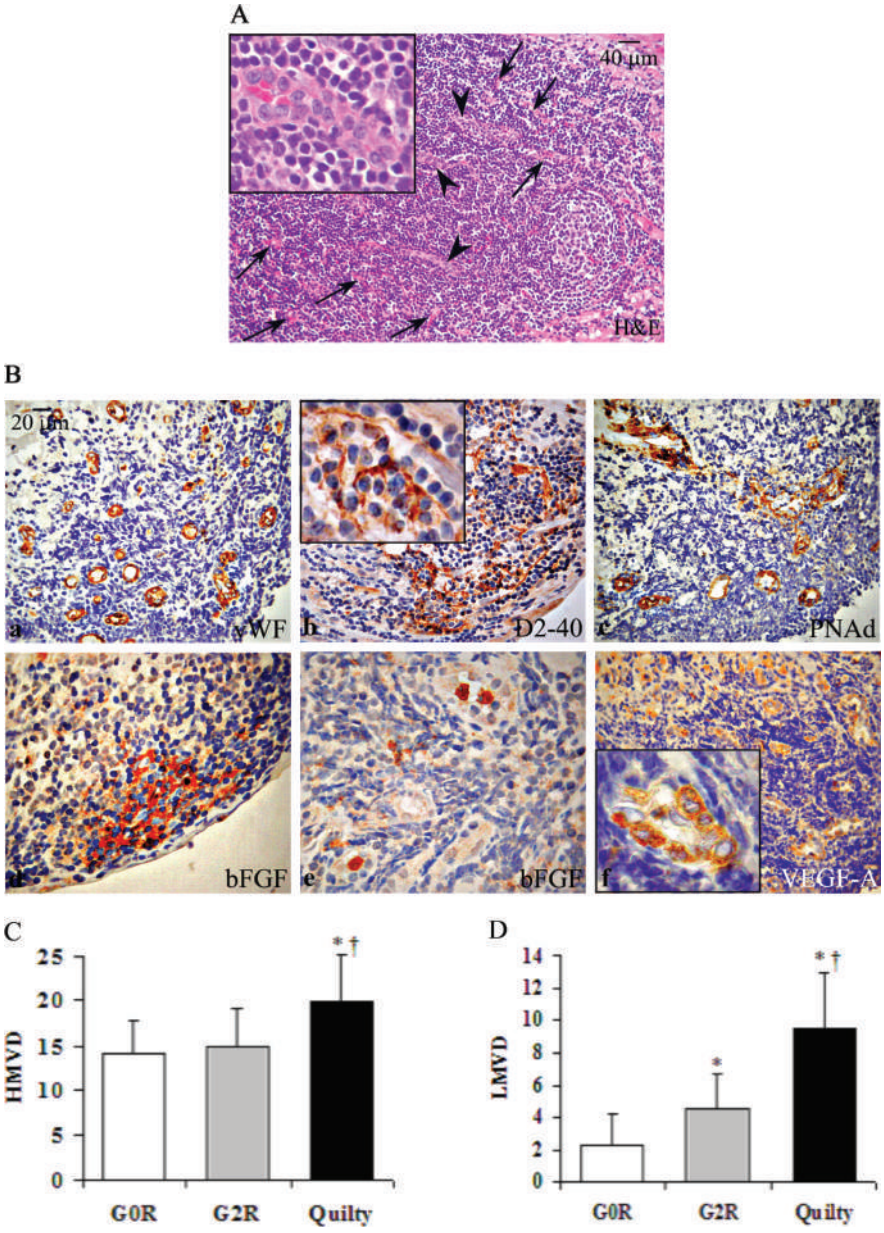

Figure 1: Morphology of QE and characterization of its hematic and lymphatic vascular networks. Panel A. QE with a distinct lymphoid follicle (down on the right) and numerous microvessels (arrows), showing, in some lengths, a cuboidal feature typical of HEV (arrowheads) (x 200) and better evidenced in the inset (x 1000). Panel B. vWF immunostaining confirms the histologic feature of high hematic microvessel density (a) and D2-40 immunostaining reveals the prominent development of lymphatics (b) draining numerous lymphocytes (inset). Endomyocardial homing of these lymphocytes is also associated with PNAd expression by HEV-like vessels (c). Vascular development is concomitant with local expression of bFGF by leukocytes (d) or cytoplasm-rich cells (probably APC) close to microvessels (e) and expression of VEGF-A (f) by most of the plumped endothelium (inset). (Panel B, a–f: ×400; insets in b and f: ×1000). Panel C. Mean ± SD of hematic microvessel (HMVD) density in groups of EMB with G0R, G2R or QE. Panel D. Mean ± SD of lymphatic microvessel (LMVD) density in groups of EMB with G0R, G2R or QE. In panels C and D: $p < 0.001$ One-way ANOVA for comparisons between 3 groups; *$p < 0.05$ Tukey-test compared with G0R; †$p < 0.05$ Tukey-test compared with G2R.

QE (12/14) were from patients (8/14) who developed recurrent G2R episodes and (c) germinal center-like structures were detected in seven. An immunopathological comparison was made of 20 QE (10 with and 10 without a distinct follicular arrangement) chosen independently from a concomitant G0, G1R or G2R and 20 EMBs with G0R, G1R or G2R (G3R were excluded because of the limited number of biopsies available).

High microvessel density in the QE is associated with angiogenesis and lymphangiogenesis

Focal microvascularization of the QE was corroborated by anti-CD31 and anti-vWF immunostaining of endothelial blood vessels (Figure 1, panel B, a). To assess whether this angiogenesis is typical of the QE we next compared the hematic microvessel density of the QE with that of G0R, G1R or G2R EMBs and found that the former was 19.8 ± 5.3 (at ×400) (no substantial differences in vessel count emerged between QE with and without follicular lymphocyte arrangement) versus 14.1 ± 4.2 of G0R, while G1R or G2R did not display any appreciable alteration in hematic microvessel density (Figure 1, panel C). Thus, we investigated whether key angiogenic factors, as bFGF and VEGF, were locally produced to stimulate vessel formation. We found that bFGF was expressed by many leukocytes forming the QE, as represented in Figure 1, panel B, d, or localized in the abundant cytoplasm of macrophage-like

mononuclear cells (Figure 1, panel B, e), while VEGF165, the most common isoform of VEGF-A, was clearly detected in the plumped endothelium (Figure 1, panel B, f and inset). Both bFGF and VEGF-A were scanty to undetectable in the G2R infiltrates and in G0R EMBs. Since VEGF-A has also demonstrated lymphatic growth factor property (19), and since the dense lymphoid aggregate of QE supposes an efficient lymphatic drain, we next assessed whether lymphatic vessel growth took place in QE.

Immunostaining with anti-D2-40 Ab, which recognizes a membrane glycoprotein whose expression is regulated by the PROX1 gene (20), revealed a prominent lymphatic sprouting of branches stacked with lymphocytes (Figure 1, panel B, b and inset). Lymphatic capillaries were present with a target like arrangement in B–T cell clustered infiltrates, and were evenly distributed and slightly less developed in the disorganized lymphoid infiltrates (with no substantial differences). The lymphatic microvessel density was 9.4 ± 3.6 in QE (Figure 1, panel D) and 4.5 ± 2.2 in the G2R infiltrate, whose minimal lymphangiogenesis (Figure 1, panel D and Figure 2, panel A, a) was absent in G1R (Figure 1, panel D and Figure 2, panel A, b). Lymphatics were either absent in G0R (Figure 1, panel D and Figure 2, panel A, c) or detectable in the interstitium (inset) depending on the biopsy section and size (G0R = 2.4 ± 2.0).

The significant ($p < 0.05$) lymphangiogenesis observed in QE lead us to assess the local production of VEGF-C. This cytokine was moderately to strongly expressed by plumped vessels and infiltrating cells in QE with or without follicles, as shown in Figure 2, panel A, d, but undetectable or barely expressed in G2R infiltrate and always undetectable in G0R EMBs.

Expression of adhesion molecules by Quilty infiltrate and lymph node addressins by Quilty microvessels

The frequent HEV-like feature displayed by Quilty microvessels prompted us to investigate the expression of PNAd, a set of sialomucins constitutively displayed on postcapillary HEV in the secondary lymphoid organs, where they mediate lymphocyte homing. Peripheral lymph node addressin (PNAd) expression was found on HEV-like vessels (which negatively stained for mucosal addressin cell adhesion molecule**,** MAdCAM, data not shown) in all QE (Figure 1, panel B, c) and was moderate to strong (Figure 2, panel B, a). It was absent in G0R and G1R and weak in G2R EMB (Figure 2, panel B, b–d). Furthermore, we looked for the expression of endothelial adhesion molecules, such as ICAM-1 and VCAM-1, which may cooperate in the focal lymphocyte extravasation typical of the QE. Interestingly, we observed a strong and diffuse ICAM-1 expression, not by microvessels, but by most Quilty-forming leukocytes

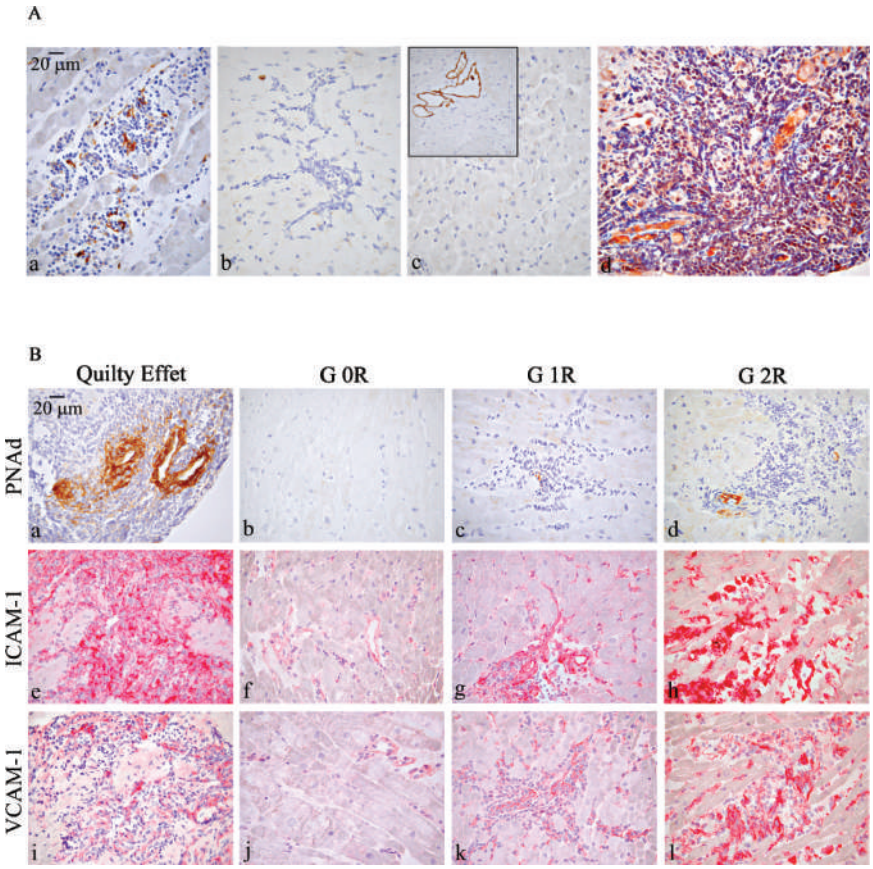

Figure 2: Lymphatic vessel distribution in G0, G1R and G2R, expression of VEGF-C in QE (panel A) and expression of adhesion molecules in different grades of AR and in QE (panel B). Panel A. Minimal lymphangiogenesis (anti-D2-40 immunostaining) was observed in the inflammatory foci of G2R (a) and it was absent in G1R (b). In G0R lymphatics may be absent (c) or detectable (inset in c) in the wider interstitium within groups of cardiomyocytes. Expression of VEGF-C by plumped vessels and infiltrating leukocytes in QE (d) (a–d: ×400). Panel B. Expression of PNAd is strong and frequent in most QE (a), while it was absent in G0R (b) and G1R (c) and occasional and scanty in G2R (d). In QE, ICAM-1 is strongly expressed on lymphomononuclear cells (e) and VCAM-1 is fairly expressed on cells endowed with elongated dendritic processes (i). By contrast, G0R usually shows a patchy, low expression of ICAM-1 (f) and a scanty expression of VCAM-1 (j), mainly by microvessels. Endothelial expression of both ICAM-1 (g) and VCAM-1 (k) is moderate in G1R and usually strong in G2R EMBs (h and l). (a–k: ×400).

(Figure 2, panel B, e), while VCAM-1 was mostly expressed by elongated dendritic processes arranged in delicate networks inside lymphoid follicles or scattered within lymphocytes lacking distinct clustering (Figure 2, panel B, i). Normal heart microvessels (EMB with G0R) usually show patchy, low expression of ICAM-1 and absent to scanty expression of VCAM-1 (Figure 2, panel B, f and j).

Endothelial expression of both ICAM-1 and VCAM-1 increased in function of the rejection grade (Figure 2, panel B, g and k) and was usually strong in G2R EMBs (Figure 2, panel B, h and l).

CXCL13 expression is associated with lymphoid neogenesis in QE and B lymphocyte recruitment in recurrent G2R episodes

The majority (61%) of QE displayed B–T lymphocyte clustering with distinct primary B-cell follicles and development in 15.5% of these cases of secondary lymphoid follicles endowed with germinal center-like structures (Figure 3, panel A, a). Distinct B–T-cell compartmentalization was not evident in the remaining QE (Figure 3, panel A, e). Immunophenotypical analyses of Quilty-forming leukocyte subsets with much the same number of cells, though differently distributed between QE with and without follicular arrangement, apart from the CD138 plasma cells that are usually more frequent in the presence of reactive follicles, revealed an infiltrate (Figure 3, panel A, b and f), mainly composed of $CD3^+$T lymphocytes (at ×400) ($CD4^+ = 94.0 \pm 10.3$; $CD8^+ = 51.4 \pm 6.2$) ($CD4^+/CD8^+$ T-cell ratio = 1,8) (Table 4). In the case of B–T-cell segregation, these cells formed a broad ring that surrounded and penetrated the inner $CD20^+$B cell area ($CD20^+ = 70.3 \pm 9.5$) (Figure 3, panel A, c and g). $CD20^+$B lymphocytes were the second most represented population, while $CD138^+$ plasma cells (their mature form) were few (8.8 ± 3.7 vs. 0.0 ± 0.0 in G0R). When reactive follicles were evident, these cells were mostly scattered in the mantle zone, which also harbors numerous CD209 (DC-$SIGN^+$) DC (mostly immature phenotype, since the antibody primarily detects immature DC) (20.4 ± 5.7 vs. 10.0

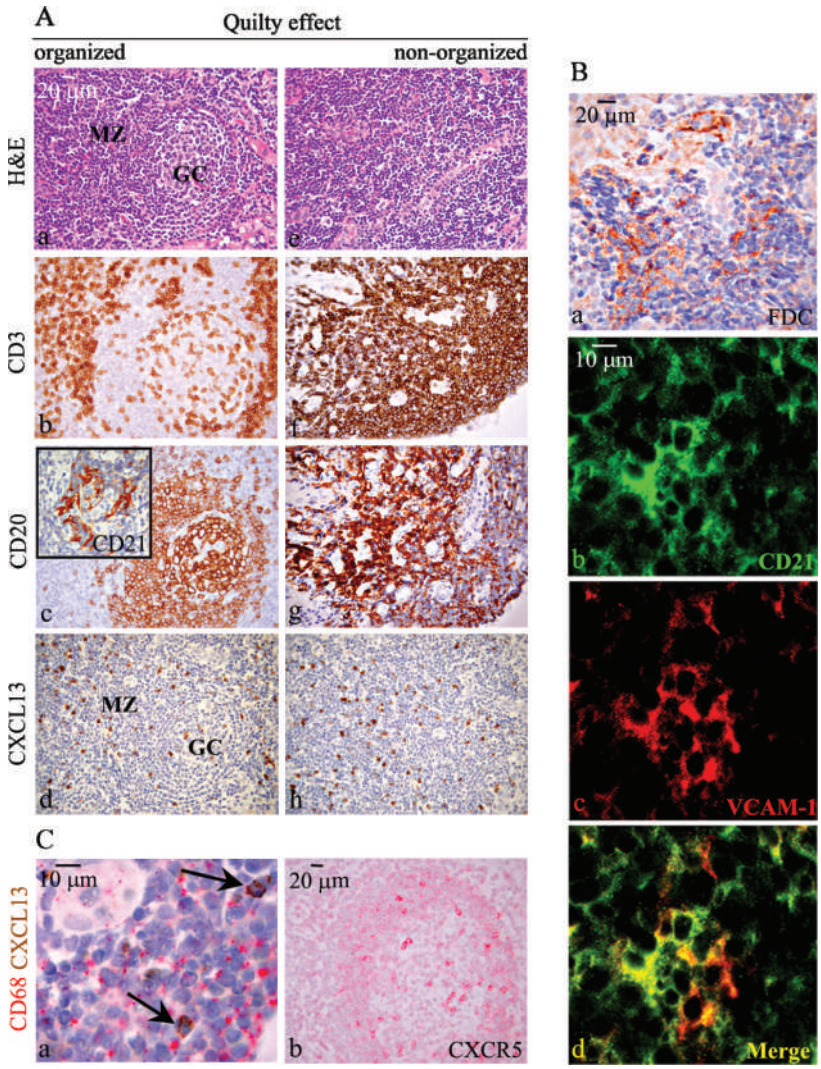

Figure 3: Morphological and immunohistochemical features of QE. Panel A. Most quilty-forming lymphocytes (a) are organized into follicles that may develop germinal centers (GC) with centroblasts and centrocytes and a peripheral mantle zone (MZ) (a). This zone is surrounded and infiltrated by a ring of $CD3^+$T cells (b) some of which penetrate the inner $CD20^+$B cell aggregate (c) enriched in $CD21^+$FDC (inset in c). CXCL13 is expressed by mononuclear cells mostly scattered in the mantle zone, but also detectable within GC (d). QE may lack distinct B–T-cell areas (b) showing numerous $CD3^+$T lymphocytes (f) intermingled with and expanded over the $CD20^+$B lymphocyte area (g). Expression of CXCL13 is also found in cells scattered throughout the lymphoid aggregates (h) (a–h: ×400). Panel B. FDC immunostaining (a) outlines the dendritic reticular processes of cells interposed among non-organised lymphomononuclear cells. Confocal analysis reveals that, particularly in the follicle, $CD21^+$FDC (b, green stained) express VCAM-1 (c, red stained) as represented by the yellow color in the merge image (d). (a: ×630; b–d: ×1000) Panel C. In QE, some (arrows) $CD68^+$cells (surface red stained) express CXCL13 (cytoplasm brown stained) (a). The expression of CXCR5 is particularly evident in the mantle zone and in germinal center (b). (a: ×1000; b: ×400).

Table 4: Mean content of leukocyte subsets in groups of EMBs with Quilty effect vs. EMBs with G0R

	G0R			Quilty		
Reactive cells[a]	(n = 20)			(n = 20)		
CD83	0.8	±	0.2	3.1	±	2.0[b]
CD209	10.0	±	2.0	20.4	±	5.7[b]
CD68	4.0	±	1.6	38.4	±	6.6[b]
CD4	1.7	±	0.2	94.0	±	10.3[b]
CD8	2.8	±	1.5	51.4	±	6.2[b]
CD20	0.7	±	0.5	70.3	±	9.5[b]
CD138	0.0	±	0.0	8.8	±	3.7[b]
CD57	0.7	±	0.4	6.8	±	2.5[b]
CD15	0.0	±	0.0	5.1	±	2.3[b]

[a]Reactive cells were counted by light microscopy, at ×400 in a 85 431.59 μm^2 field, on single immunostained formalin-fixed paraffin-embedded sections. Results are mean ± SD of positive cells/field.
[b] $p < 0.001$ Mann–Whitney *U* test vs. G0R.

± 2.0 in G0R) and $CD68^+$ macrophages (38.4 ± 6.6 vs. 4.0 ± 1.6 in G0R), and few $CD83^+$DC (mature phenotype) (3.1 ± 2.0 vs. 0.8 ± 0.2). A few $CD57^+$NK cells (6.8 ± 2.5 vs. 0.7 ± 0.4) and $CD15^+$granulocytes (5.1 ± 2.3 vs. 0.0 ± 0.0) were also detected (Table 4). A distinct network of $CD35^+/CD23^+/CD21^+$ interdigitating follicular DC (FDC) was observed inside the follicles (Figure 3, panel A, inset in c), and occasionally when distinct lymphocyte segregation was lost (Figure 3, panel B, a). Confocal analyses of tissue sections immunostained with anti-CD21/anti-VCAM-1 Abs revealed the expression of VCAM-1 by $CD21^+$FDC in the follicles (Figure 3, panel B, b–d).

The follicles and germinal centers observed in QE closely mimicked those found in secondary (lymph nodes) (Figure 4, panel A, a) and tertiary (as the mucosal associated lymphoid tissue, MALT, that can be detected in H. pylori-associated chronic gastritis) (Figure 4, panel A, b) lymphoid tissues. The development of B-cell follicles as a common morphological feature raised the question of whether B-cell homing molecules, such as CXCL13 and B-cell activating factor of the tumor necrosis factor family, BlyS/BAFF, were also expressed in QE. BlyS/BAFF was always undetectable in the Quilty samples, whereas CXCL13 was constantly and clearly expressed.

In QE with secondary follicles, therefore, CXCL13 was mostly produced by $CD68^+$ cells (Figure 3, panel C, a) scattered in the mantle zone and also detectable in germinal centers (Figure 3, panel A, d), as in lymph node or gut MALT (Figure 4, panel A, c and d, respectively). In QE lacking distinct B–T cell clustering or germinal center formation, it was scattered throughout the aggregates (Figure 3, panel A, h). Its expression appeared a little more frequent in the presence of clear germinal center formation.

Expression of CXCR5, the ligand of CXCL13, by small lymphocytes was weak to undetectable in the absence of distinct clustering, whereas it was found in the mantle zone and, occasionally, in germinal centers in QE containing reactive follicles (Figure 3, panel C, b).

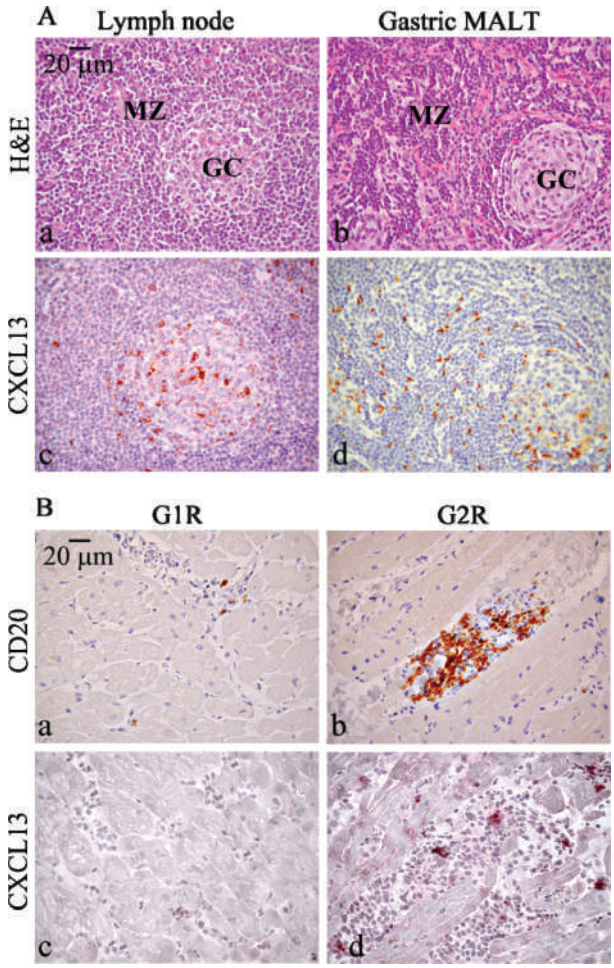

Figure 4: Morphological and immunohistochemical features of lymph node and gastric MALT in panel A, and of G1R and G2R in panel B. Panel A. Lymph node (a) and gastric MALT (b) show reactive follicles endowed with germinal center (GC) and mantle zone (MZ) and related expression of CXCL13 in c and d. (a–d: ×400) Panel B. In contrast with QE, both B lymphocytes (a) and expression of CXCL13 (c) are absent in G1R, while in some G2R EMBs a small cluster of B cells (b) is detected in association with a low, but distinct CXCL13 expression (d) by a few cytoplasm-rich APC-like cells. (a–d: ×400).

CXCL13 was undetectable in G0R and G1R EMBs, which were usually devoid of $CD20^+$B cells (Figure 4, panel B, a and c), whereas it was clearly expressed by a few APC-like cells found in EMBs from 8/14 patients who developed G2R with a distinct $CD20^+$B infiltrate (Figure 4, panel B, b and d). These biopsies tested negative for enterovirus, cytomegalovirus and Epstein–Barr virus infections, i.e. the most common viral co-factors of inflammatory reactions. They were also negative for C4d and C3d, thus ruling out

humoral rejection as a cause of the B-cell infiltrate. These B-cell-rich G2R EMBs were from five patients who had two rejection episodes and three who had three episodes, and had been assigned to a high-risk allograft rejection group (13) to distinguish them from patients (6/14) with only one G2R episode during the year.

Discussion

The 'QE' has been poorly investigated and ignored too long by cardiologists and immunologists presumably because it does not give rise to clinical symptoms and does not appear to impair a patient's health. Since several studies have illustrated the multi-faceted function of a leukocyte infiltrate in cancer (21,22), autoimmunity (23,24) and allograft rejection (13), it would be strange if the infiltrate forming the QE were found to be devoid of a substantial biological meaning, especially because its relationship with both acute (2,3) and chronic (4) allograft rejection have been strongly suggested. Understanding the pathobiology of the QE may help to address this issue. Taking the histopathological analyses as a starting point, we searched for cellular and molecular events involved in the onset of QE and tested the hypothesis of whether they should be the same as those leading to lymphoid neogenesis and whether they should be, at least in part, shared with those governing AR episodes. Our data indicate that in the majority (about 61%) of QE arrangement of lymphocytes in well-defined VCAM-1^+FDC containing B-cell follicles (sometimes developing germinal center-like structures) and DC-rich T-cell areas closely follows the secondary and tertiary lymphoid tissue microarchitecture. The remaining QE, though lacking this structure, may harbor a delicate FDC web suggesting that germinal center-like B-cell responses may develop within the aggregates (25). During our revision of the initial version of the present manuscript, Sattar et al. reported their observation of the $CD21^+$FDC network in most of QE. They proposed it as diagnostic tool in differentiating QE from AR (26) and suggested that QE has a typical lymphoid-like tissue organization. Lymphoid follicles and apparent germinal center formation in Quilty lesions have already been described (5–7). McManus reported a QE that contained proliferating B cells arranged in germinal centers and was preceded by repeated QE (7). The data gathered so far extend to the human heart allograft the concept of ectopic lymphoid follicle as an immunomorphological response to chronic local antigen (in this case, alloantigen) stimulation (24). As observed by Luthringer et al. (6), we found that most EMBs with G2R displayed a concomitant QE, in addition, these QE frequently showed germinal center-like structures in EMBs from patients with recurrent AR. Though the number of patients enrolled may be stated as a limitation of our study, a previous work of more than 5000 EMBs (27) by Costanzo et al. demonstrated that patients who develop a QE in the presence or absence of rejection more frequently undergo AR later. Thus, some biological pathways are probably shared by QE and AR as indicated finding of CXCL13 and its receptor CXCR5 as molecular determinants associated with both the QE, particularly QE showing germinal centers, and AR, particularly the recurrent AR marked by distinct B lymphocyte infiltrates (13). Evidence of B lymphocytes in AR has been reported (28,29), with variable results depending on the methods. Our group recently reported that most AR biopsies showed a very low or absent B-cell content and that a discrete B infiltrate was indicative of a high risk of rejection recurrence (13). We here suggest the involvement of CXCL13 in their endomyocardial recruitment.

In QE the main source of CXCL13, as reported for rheumatoid arthritis and ulcerative colitis (30), is $CD68^+$cells. These are well represented in QE, though cooperation by small lymphocytes cannot be ruled out. CXCL13 is one of the most important B-cell chemoattractants (31) and essential for the complex architecture of lymphoid organs and the interaction of B and T cells in lymph follicles. B cells are second to $CD4^+$T cells in their contribution to QE formation and are tightly intermingled with them, whereas they are exceptionally detected in G2R infiltrate in concomitance with repeated AR episodes. Accordingly, CXCL13 is firmly well expressed in QE, while its expression is scanty and uncommon in G2R infiltrates. Chronic alloantigen stimulation may thus trigger a cascade of events resulting in a strong CXCL13 production and wide, but clinically silent, lymphocyte infiltrate, i.e. the QE, or in scanty production and 'detrimental' G2 inflammatory reaction. The fine immunologic mechanisms controlling both events remain to be explored. Interestingly, the endothelial adhesion/activation molecules, VCAM-1 and ICAM-1, whose expression increases in function of the grade of rejection, are not expressed by the endothelium in the QE, but by most infiltrating leukocytes, which readily adhere to each other and sustain the lymphoid-like tissue architecture. Heart allograft can thus be added to few anatomical sites that can harbor chronic inflammatory diseases including MALT (32), rheumatoid arthritis (33) Sjögren's syndrome and Hashimoto's thyroiditis, which develop ectopic lymphoid-like tissue (24).

Lymphoid neogenesis in pericardial, subpericardial or intramyocardial sites and its correlations with chronic, rather than acute, rejection has been recently described in an experimental murine transplantation model (34). However, any attempt of comparison with findings from a clinical setting requires previous assessment of whether the lesion developed in an animal model has the meaning of endomyocardial infiltrate forming QE in humans.

Assignment of the QE as a novel tertiary lymphoid organ indicates that it is not simply inert, but an immunologically dynamic lesion, as is also demonstrated by the concomitant vessel remodeling, namely: (a) expansion of hematic and lymphatic networks, probably sustained by the local production of VEGF-A by endothelial cells or bFGF and VEGF-C by inflammatory cells (35,36), and (b)

reprogramming of the endothelial gene expression profile, since vessels acquire the cuboidal appearance and functional property of specialized HEV. In particular through induction of PNAd, while, as expected and as found in peripheral lymph node, MadCAM was lacking, since its expression likely requires a specialized cytokine microenvironment mimicking that of mesenteric lymph nodes and Payer patches or lamina propria vasculature where MadCAM is constitutively produced (37). PNAd expression by HEV enables extravasation of naïve T and B cells into lymph nodes (38), probably into heart and kidney allografts undergoing AR (39,40) and, as shown in this article, into heart allografts developing the QE. By contrast with AR, however, QE shows a strong and frequent expression of PNAd which, as observed in chronic inflammatory lesions, may lead to the abundant lymphocyte infiltrate typical of QE (41).

In conclusion, we here provide evidence that the QE displays the cellular, molecular and vascular features of lymphoid organs. Furthermore, we propose CXCL13-led B-cell recruitment as the biologic event shared by QE and recurrent AR and indicative of immunopathological links between them. These findings, together with the fact that QE is lacking in clinical signs and symptoms, suggest that it is beneficial for the immediate allograft outcome and may have a protective function by mounting a prompt, local response to long-lasting alloantigen stimulation. Comprehension of the biological events associated with the QE may shed new light on the dynamics of allograft failure.

Acknowledgments

This work is supported by a grant awarded by Fondazione Cassa di Risparmio della Provincia di Chieti (CariChieti), Italy.

A special word of thanks to Professor John Iliffe for editing the manuscript.

References

1. Joshi A. The quilty effect: Current knowledge and clinical implications. Transplant Proc 1998; 30: 907–908.
2. Smith RN, Chang Y, Houser S, Dec GW, Grazette L. Higher frequency of high-grade rejections in cardiac allograft patients after quilty B lesions or grade 2/4 rejections. Transplantation 2002; 73: 1928–1932.
3. Chu KE, Ho EK, de la Torre L, Vasilescu ER, Marboe CC. The relationship of nodular endocardial infiltrates (quilty lesions) to survival, patient age, anti-HLA antibodies, and coronary artery disease following heart transplantation. Cardiovasc Pathol 2005; 14: 219–224.
4. Yamani MH, Ratliff NB, Starling RC et al. Quilty lesions are associated with increased expression of vitronectin receptor (alphavbeta3) and subsequent development of coronary vasculopathy. J Heart Lung Transplant 2003; 22: 687–690.
5. Fishbein MC, Bell G, Lones MA et al. Grade 2 cellular heart rejection: Does it exist? J Heart Lung Transplant 1994; 13: 1051–1057.
6. Luthringer DJ, Yamashita JT, Czer LS, Trento A, Fishbein MC. Nature and significance of epicardial lymphoid infiltrates in cardiac allografts. J Heart Lung Transplant 1995; 14: 537–543.
7. Dong C, Winters GL, Wilson JE, McManus BM. Enhanced lymphocyte longevity and absence of proliferation and lymphocyte apoptosis in quilty effects of human heart allografts. Am J Pathol 1997; 151: 121–130.
8. Landis JR, Koch GG. The measurement of observer agreement for categorical data. Biometrics 1977; 33: 159–174.
9. Billingham ME, Cary NR, Hammond ME et al. A working formulation for the standardization of nomenclature in the diagnosis of heart and lung rejection: Heart rejection study group, The international society for heart transplantation. J Heart Transplant 1990; 9: 587–593.
10. Stewart S, Winters GL, Fishbein MC et al. Revision of the 1990 working formulation for the standardization of nomenclature in the diagnosis of heart rejection. J Heart Lung Transplant 2005; 24: 1710–1720.
11. McGoon MD, Frantz RP. Techniques of immunosuppression after cardiac transplantation. Mayo Clin Proc 1992; 67: 586–595.
12. Dixon MF, Genta RM, Yardley JH, Correa P. Classification and grading of gastritis. The updated Sydney system. International workshop on the histopathology of gastritis, Houston 1994. Am J Surg Pathol 1996; 20: 1161–1181.
13. Sorrentino C, Scarinci A, D'Antuono T et al. Endomyocardial infiltration by B and NK cells foreshadows the recurrence of cardiac allograft rejection. J Pathol 2006; 209: 400–410.
14. Zhang H, Li Y, Peng T et al. Localization of enteroviral antigen in myocardium and other tissues from patients with heart muscle disease by an improved immunohistochemical technique. J Histochem Cytochem 2000; 48: 579–584.
15. Plachter B, Nordin M, Wirgart BZ et al. The DNA-binding protein P52 of human cytomegalovirus reacts with monoclonal antibody CCH2 and associates with the nuclear membrane at late times after infection. Virus Res 1992; 24: 265–276.
16. Rodriguez ER, Skojec DV, Tan CD et al. Antibody-mediated rejection in human cardiac allografts: Evaluation of immunoglobulins and complement activation products C4d and C3d as markers. Am J Transplant 2005; 5: 2778–2785.
17. Jacobs JJ, Lehe C, Cammans KD, Yoneda K, Das PK, Elliott GR. An automated method for the quantification of immunostained human Langerhans cells. J Immunol Methods 2001; 247: 73–82.
18. Di Carlo E, Cappello P, Sorrentino C et al. Immunological mechanisms elicited at the tumour site by lymphocyte activation gene-3 (LAG-3) versus IL-12: Sharing a common Th1 anti-tumour immune pathway. J Pathol 2005; 205: 82–91.
19. Bjorndahl MA, Cao R, Burton JB et al. Vascular endothelial growth factor-A promotes peritumoral lymphangiogenesis and lymphatic metastasis. Cancer Res 2005; 65: 9261–9268.
20. Schacht V, Dadras SS, Johnson LA, Jackson DG, Hong YK, Detmar M. Up-regulation of the lymphatic marker podoplanin, a mucin-type transmembrane glycoprotein, in human squamous cell carcinomas and germ cell tumors. Am J Pathol 2005; 166: 913–921.
21. Di Carlo E, Forni G, Lollini P, Colombo MP, Modesti A, Musiani P. The intriguing role of polymorphonuclear neutrophils in antitumor reactions. Blood 2001; 97: 339–345.
22. de Visser KE, Eichten A, Coussens LM. Paradoxical roles of the immune system during cancer development. Nat Rev Cancer 2006; 6: 24–37.
23. Airoldi I, Di Carlo E, Cocco C et al. Lack of IL12rb2 signaling predisposes to spontaneous autoimmunity and malignancy. Blood 2005; 106: 3846–3853.
24. Aloisi F, Pujol-Borrell R. Lymphoid neogenesis in chronic inflammatory diseases. Nat Rev Immunol 2006; 6: 205–217.

25. Lindhout E, Koopman G, Pals ST, de Groot C. Triple check for antigen specificity of B cells during germinal centre reactions. Immunol Today 1997; 18: 573–577.
26. Sattar HA, Husain AN, Kim AY, Krausz T. The presence of a CD21$^+$ follicular dendritic cell network distinguishes invasive quilty lesions from cardiac acute cellular rejection. Am J Surg Pathol 2006; 30: 1008–1013.
27. Costanzo-Nordin MR, Winters GL, Fisher SG et al. Endocardial infiltrates in the transplanted heart: Clinical significance emerging from the analysis of 5026 endomyocardial biopsy specimens. J Heart Lung Transplant 1993; 12: 741–747.
28. Radio SJ, McManus BM, Winters GL et al. Preferential endocardial residence of B-cells in the "quilty effect" of human heart allografts: Immunohistochemical distinction from rejection. Mod Pathol 1991; 4: 654–660.
29. Michaels PJ, Kobashigawa J, Laks H et al. Differential expression of RANTES chemokine, TGF-beta, and leukocyte phenotype in acute cellular rejection and quilty B lesions. J Heart Lung Transplant. 2001; 20: 407–416.
30. Carlsen HS, Baekkevold ES, Morton HC, Haraldsen G, Brandtzaeg P. Monocyte-like and mature macrophages produce CXCL13 (B cell-attracting chemokine 1) in inflammatory lesions with lymphoid neogenesis. Blood 2004; 104: 3021–3027.
31. Legler DF, Loetscher M, Roos RS, Clark-Lewis I, Baggiolini M, Moser B. B cell-attracting chemokine 1, a human CXC chemokine expressed in lymphoid tissues, selectively attracts B lymphocytes via BLR1/CXCR5. J Exp Med 1998; 187: 655–660.
32. Mazzucchelli L, Blaser A, Kappeler A et al. BCA-1 is highly expressed in Helicobacter pylori-induced mucosa-associated lymphoid tissue and gastric lymphoma. J Clin Invest 1999; 104: R49–54.
33. Shi K, Hayashida K, Kaneko M et al. Lymphoid chemokine B cell-attracting chemokine-1 (CXCL13) is expressed in germinal center of ectopic lymphoid follicles within the synovium of chronic arthritis patients. J Immunol 2001; 166: 650–655.
34. Baddoura FK, Nasr IW, Wrobel B. Lymphoid neogenesis in murine cardiac allografts undergoing chronic rejection. Am J Transplant 2005; 5: 510–516.
35. Gannon G, Mandriota SJ, Cui L, Baetens D, Pepper MS, Christofori G. Overexpression of vascular endothelial growth factor-A165 enhances tumor angiogenesis but not metastasis during beta-cell carcinogenesis. Cancer Res 2002; 62: 603–608.
36. Alitalo K, Tammela T, Petrova TV. Lymphangiogenesis in development and human disease. Nature 2005; 438: 946–953.
37. Briskin M, Winsor-Hines D, Shyjan A et al. Human mucosal addressin cell adhesion molecule-1 is preferentially expressed in intestinal tract and associated lymphoid tissue. Am J Pathol 1997; 151: 97–110.
38. Rosen SD. Endothelial ligands for L-selectin: From lymphocyte recirculation to allograft rejection. Am J Pathol 1999; 155: 1013–1020.
39. Toppila S, Paavonen T, Nieminen MS, Hayry P, Renkonen R. Endothelial L-selectin ligands are likely to recruit lymphocytes into rejecting human heart transplants. Am J Pathol 1999; 155: 1303–1310.
40. Kirveskari J, Paavonen T, Hayry P, Renkonen R. De novo induction of endothelial L-selectin ligands during kidney allograft rejection. J Am Soc Nephrol 2000; 11: 2358–2365.
41. Kobayashi M, Mitoma J, Nakamura N, Katsuyama T, Nakayama J, Fukuda M. Induction of peripheral lymph node addressin in human gastric mucosa infected by Helicobacter pylori. Proc Natl Acad Sci U S A 2004; 101: 17807–17812.